Traits of bulk Pu phases in Pb-Pu superlattice phases from first principles

Sven P. Rudin
Los Alamos National Laboratory, Los Alamos, New Mexico 87545, USA
(Received 24 July 2007; revised manuscript received 10 October 2007; published 16 November 2007)

Density functional theory calculations allowing spin polarization predict two phases in Pb-Pu superlattices. One phase exhibits bond lengths similar to bulk α-Pu and a degree of localization of $5f$ electron states corresponding to bulk β-Pu, while for the other phase, these take on values like those found in bulk δ-Pu. The superlattice geometry localizes the $5f$ electron states mainly in planes perpendicular to the stacking direction. The disparate volumes between phases found in bulk Pu also emerge in Pb-Pu superlattices. The structures of the two phases differ in the presence of pairing between neighboring Pu planes. The paired and unpaired phases can coexist in special cases. The simple geometry of the pairing allows for detailed calculations to explore the transition along the complete path connecting the two phases; to date, the bulk phases have evaded such an examination. In Pb-Pu superlattices, the localization of $5f$ electron states smoothly parallels changes in geometry, in accordance with tendencies that emerge in bulk Pu calculations. Changing the layer thicknesses affects the ordering of the energies of the two phases for stacking along the (001) and (111) directions. For stacking in the (011) direction, only one phase appears with very weakly paired Pu planes. Compared to bulk Pb and Pu, the superlattices with single-monolayer thicknesses appear energetically favorable; pilot calculations suggest that thicker layers become energetically favorable with interface alloying.

DOI: 10.1103/PhysRevB.76.195424 PACS number(s): 61.46.−w, 68.65.Cd, 71.27.+a, 71.28.+d

I. INTRODUCTION

Recent calculations predict that Pb-Pu superlattices form nanostructures with two competing phases strongly related to the two most important phases of bulk plutonium.[1] This result suggests furnishing actinide materials with nanoscale structures as an avenue toward improved scientific understanding and greater technological control of actinide material characteristics. These characteristics include unique crystal structures,[2] Mott transitions,[3–6] strong anharmonicity,[7–10] and strong electron-phonon coupling.[11] In particular, the Mott transition wherein $5f$ electronic states shift from itinerant to localized emerges as a driver of many of the other properties. The scientific importance of the two bulk Pu phases mentioned above stems from their sitting on opposite sides of this transition: some of the all-itinerant $5f$ electron states in the low-temperature, monoclinic α phase become localized in the high-temperature, face-centered cubic (fcc) δ phase.

Investigations into connections between the two bulk Pu phases suffer from the lack of an unambiguous geometric connection between the two crystal structures. The 16-atom unit cell of the α phase shows significantly reduced symmetry compared to the cubic symmetry of the single-atom unit cell of the δ phase. To date, no distinct transformation path linking the two structures has emerged. In contrast, the two phases in Pb-Pu superlattice transform into each other by an easily described distortion, the pairing of Pu planes (visually apparent in Fig. 1).[1] This pairing occurs accompanied by a volume collapse and a delocalization of the $5f$ electrons along the lines of the Mott transition associated with the bulk phases. Furthermore, the bond lengths between Pu atoms in the paired phase take on values very close to the short and long bonds of α-Pu, while the bond lengths between Pu atoms in the unpaired phase take on values very close to those in δ-Pu.

The similarities between corresponding bulk and superlattice phases suggest that nanostructures could be used to tailor the $5f$ electron localization, effectively fine-tuning the associated properties. The simple geometric transformation in the superlattices encourages their use to study the transformation in a more controllable manner. To this end, this work extends the recent calculations to explore Pb-Pu superlattices in more detail.

The previous study placed n_{ML} monolayers (ML) of fcc Pu next to the same number n_{ML} of fcc Pb ML in the (001) direction;[1] here, investigations also include stacking in the (011) and (111) directions. The paired phase discovered in the earlier study appeared when spin polarization was not permitted (see Sec. II); here, optimization starting from this phase's geometry while allowing spin polarization leads to a lower energy phase that retains the pairing simultaneously with the Pu atoms acquiring spin moments. The work presented here includes a detailed exploration of the path connecting this phase with the unpaired phase; the result reveals

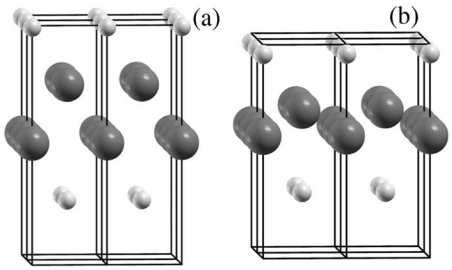

FIG. 1. Geometries of (001)-direction Pb-Pu superlattices with two monolayers of Pb and of Pu (n_{ML}=2) in the (a) unpaired and (b) paired phases. Small and large spheres represent Pb and Pu atoms, respectively; rods delineate the simulation cells (four shown for each case). The transition between the two phases involves a simple change of geometry where the two Pu monolayers move toward each other.

a smooth change of the electronic structure with the change of geometry (the pairing of Pu planes).

Geometry drives the choice to use Pb: of all elemental fcc metals, Pb exhibits the closest lattice parameter to that of fcc Pu (6.5% mismatch). To date, Pb-Pu superlattice samples have not been made. Experimentally, the two metals have been examined together in the solid state for their alloying properties.[12] Theoretically, the two metals are predicted to form a perfect, *spdf*-like 32-electron molecular system.[13] Varying degrees of electron localization have been seen experimentally in thin Pu layers deposited on Mg.[14]

II. METHOD

A. Exploiting spin polarization to emulate electron-electron correlation

Solid plutonium's encompassing of both localized and itinerant 5*f* electrons make it challenging for solid state electronic structure methods. For most materials, the majority of such successful methods implement density functional theory[15] (DFT) with approximate treatment of exchange and correlation such as the local density approximation[16] (LDA) and the generalized gradient approximation (GGA).[17] DFT in the GGA produces results in good agreement with experimental structural data for the α phase of bulk Pu. The presence of localized 5*f* electrons in the δ phase requires enhancements to the GGA. Successful approaches to treat the variable 5*f* localization include GGA methods enhanced with a split 5*f* manifold in the mixed level model[18] and in the self-interaction corrected LDA[19,20] or with an on-site Hubbard parameter in LDA+*U* (Refs. 21–23) and dynamical mean field theory.[24] Similar success stems from GGA calculations, where the local spin density replaces the local charge density, i.e., through the introduction of magnetic moments by allowing spin polarization.[5,25–28]

The work described here results from DFT calculations in the GGA performed allowing spin polarization to emulate the effects of electron-electron correlation in localized 5*f* electron states. This approach successfully describes the equilibrium volumes and bulk moduli of bulk Pu,[28] which has sparked a debate as to whether high-temperature Pu phases are magnetic; to date, no magnetic moment has been experimentally observed.[29] The procedure cannot reproduce the large electronic specific-heat coefficient of fcc Pu, i.e., not all physical properties of Pu are adequately described. Nonetheless, the approach also replicates the equilibrium structures and energetics of Pu compounds[30] and alloys,[31,32] and hence, serves as an appropriate method of investigating the equilibrium structures and energetics of Pb-Pu superlattices.

Refinements to this approximate treatment, orbital polarization and spin-orbit coupling, are not included here. In that sense, this work sacrifices higher accuracy in the interest of investigating a broader range of systems. More accurate treatments for systems of particular interest may alter the specific values of, e.g., energy differences and equilibrium lattice constants, but in all likelihood not affect the conclusions.

B. Vienna *ab initio* simulation package

The DFT framework used here comprises the projector-augmented wave (PAW) method[33] implemented in the Vienna *ab initio* simulation package (VASP).[34,35] All electrons appear in the PAW method as either adaptable in valence states or frozen in atomic core states. Of the potentials supplied with VASP, this work uses those that treat as valence electrons for Pb the 6*s* and 6*p* valence states, and for Pu, the 6*s* and 6*p* semicore and the 5*f*, 6*d*, 7*s*, and 7*p* valence states. The Pu semicore states are included due to the short Pu-Pu bonds that appear between paired Pu planes; bonds involving Pb atoms remain close to the Pb-Pb bond length of equilibrium bulk fcc Pb, so the Pb semicore 5*d* electrons are treated as core states (geometries and energy differences among small Pb-Pu superlattice systems change negligibly when the valence space includes the 5*d* electrons). The PAW sphere radii are 1.69 and 1.57 Å for Pb and Pu, respectively, which lead to no overlap between spheres with the exception of a small overlap between Pu atoms for some of the shortest bonds. The PAW potentials use six and eight nonlocal projectors for Pb and Pu, respectively; the plane wave energy cutoff is set to 320 eV, which converges energy differences to well below 1 meV/atom. Exchange and correlation are treated in the GGA with the functional of Perdew and Wang (PW91).[36,37] For each system, the *k*-point mesh is refined until the total energy (calculated using the linear tetrahedron method with the corrections[38] of Blöchl *et al.*) converges within 1 meV/atom.

C. Optimization procedure

Unless specifically stated, optimization of the superlattices starts from the same basic pattern. The initial geometry consists of n_{ML} monolayers of fcc Pb stacked on n_{ML} monolayers of fcc Pu in one of the three high-symmetry directions. The unit cell contains one atom per monolayer. Cell parameters, atomic positions, and spin moments undergo concurrent optimization.

As the superlattices are optimized, their magnetic moments are either kept at zero or are allowed to vary. Without moments, the systems remain nonmagnetic (NM). In previous work, two magnetic structures were used to seed the calculations: a ferromagnetic (FM) arrangement and an antiferromagnetic (AFM) arrangement within the Pu layer along the stacking direction. This work omits FM arrangements because they lead to results similar to those of AFM arrangements, but with slightly higher energy. During optimization of the superlattice structures, the magnetic moments keep their sign while changing their magnitude. The Pb atoms consistently end up with a moment of zero.

D. Phonons

Calculations of phonon frequencies result from applying the direct force method.[39–42] The method evaluates the force constants in large simulation cells consisting of repeated unit cells from the forces on all atoms calculated in response to the displacement of the basis atom in one unit cell. A spatial Fourier transform with a given wave vector **q** of the force

constants results in the **q**-dependent dynamical matrix. Diagonalization of the dynamical matrix gives the corresponding frequencies.

The calculations needed for converged phonon dispersions can become quite large. Long-range forces require large simulation cells. Systems with forces that are sensitive to the electronic wave function require a fine k-point mesh. As described below, the phonons calculated here serve to investigate the relative thermal stability of two phases. The quantity of interest is the free energy, which depends on integrals over the phonon density of states (DOS), i.e., is much less sensitive to details of the phonon dispersion. Since the intention here is to search for striking rather than subtle differences in the phonons, a relatively small supercell with 16 atoms suffices. This supercell yields frequencies at the center and high-symmetry edge points of the Brillouin zone that are precise (within the approach used to calculate the forces), and frequencies at other points that are approximate. The calculated forces converge with a k-point mesh of $6\times6\times6$. To improve convergence, the force calculations employ a Fermi smearing with a width of 0.2 eV.

III. RESULTS

A. Stable PbPu alloy as superlattice with $n_{ML}=1$

The energies of the optimized AFM (001)-direction Pb-Pu superlattices lie 0.02–0.06 eV/atom above a reference energy obtained by averaging the calculated values for bulk fcc Pb and bulk fcc Pu (with AFM magnetic structure). The exception appears for $n_{ML}=1$, where two structures exist with different c/a ratios and lie 0.21 eV/atom ($c/a=0.97$) and 0.16 eV/atom ($c/a=0.54$) lower than the bulk average. These superlattices correspond to a PbPu alloy in tetragonal distortions of the B2 structure (the undistorted, cubic B2 alloy has a higher calculated energy 0.11 eV/atom below the bulk average). The two structures have similar volumes, 27.93 and 28.15 Å^3, as well as similar spin moments on the Pu atom, $5.4\mu_B$ and $5.3\mu_B$, indicating a similar degree of $5f$ electron localization.

For $n_{ML}=1$, i.e., Pu and Pb layers of monatomic thickness, the single Pu atom in the unit cell and, therefore, all Pu atoms in the superlattice have their spin in one particular direction. Increasing the unit cell allows for Pu spin moments that alternate their sign. Doubling the unit cell in the stacking direction, i.e., allowing interlayer AFM magnetic structure, is energetically less favored. Doubling the unit cell perpendicular to the stacking direction allows for Pu spin moments that alternate their sign within the monolayer. For the energetically less-favored structure (with $c/a=0.54$), an in-plane AFM structure in the (100) direction lowers the energy slightly (by 16 meV/atom), while an in-plane AFM structure in the (110) direction does not. No in-plane AFM structure lowers the energy of the energetically favored structure (with $c/a=0.97$).

The two $n_{ML}=1$ structures differ in energy by 47 meV/atom. This energy difference approaches room temperature within a factor of 2, which raises the possibility of a temperature-induced phase transition. In order for temperature to induce the phase transition, it would have to push the free energy of the structure with $c/a=0.54$ below that of the structure with $c/a=0.97$. A large difference in the free energies' rate of change with temperature requires strongly different phonon excitation spectra.

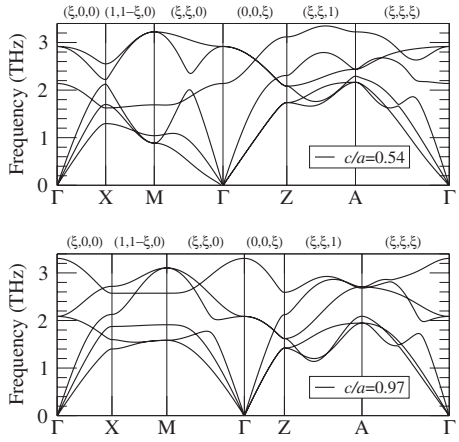

FIG. 2. Calculated phonon dispersion for $n_{ML}=1$ (001)-direction Pb-Pu superlattices. The simple tetragonal lattice with $a=b\neq c$ yields the following high-symmetry points in reciprocal space (given in units of π/a, π/a, and π/c, respectively): Γ (000), X (100), M (110), Z (001), and A (111). The phonon frequencies are plotted along paths of high-symmetry directions perpendicular (Γ-X-M-Γ) and parallel (Γ-Z) to the stacking direction as well as along the diagonal (Γ-A).

Figure 2 compares the calculated phonon dispersions for the two $n_{ML}=1$ structures. The ordering of the frequencies of the optical modes at Γ reflects the change in the c/a ratio. For $c/a=0.97$, the single mode with amplitude in the stacking direction appears much stiffer than the two modes that vibrate perpendicular to the stacking direction. This ordering corresponds to the phonon dispersion of typical fcc-like crystal (where $c/a=1$). Changing to $c/a=0.54$ reverses this ordering: the tetragonal compression makes the Pu-Pb bonds largely horizontal, making vibrational modes perpendicular to the stacking direction stiffer and those parallel to it softer. The same type of softening appears for the two transverse modes for wave vectors in the $(\xi,\xi,0)$ direction, while the corresponding longitudinal mode stiffens.

While the two spectra differ in such details, overall they span a very similar frequency range. The two structures will differ little in the thermal contributions to the free energy from the phonons, i.e., not enough to overcome the 47 meV/atom difference. Since the phonons cannot produce a phase transition, none is expected to occur. Other sources contribute too little to the free energy, e.g., that due to electronic excitations. For completeness, Fig. 3 shows the electronic DOS for the two geometries.

Without a phase transition, the structure with $c/a=0.97$ remains more stable. For $c/a=1$, this structure corresponds to the $L1_0$ (AuCu) structure. The $L1_0$ structure appears as a very stable alloy among fcc superstructures in the Pu-Ga system, where chemical short-range-order effects stabilize fcc superstructure solid solutions.[32] How chemical short-range-order effects affect the Pb-Pu system will require further investigations.

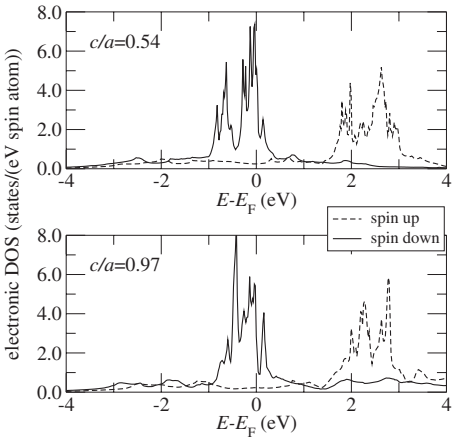

FIG. 3. Calculated electronic DOS for $n_{ML}=1$ (001)-direction Pb-Pu superlattices. The DOS in the range around the Fermi energy E_F consists almost entirely of localized Pu $5f$ electron states.

In summary, for $n_{ML}=1$, no pairing occurs and the superlattice, in fact, corresponds to an alloy with tetragonally distorted B2 crystal structure. The tetragonal distortion stabilizes the crystal at two values of c/a with energies well below the bulk average. The weaker distortion of the B2 structure emerges as more stable at low temperatures and from comparisons of phonon frequencies is expected to remain more stable at higher temperatures.

B. (001) stacking direction with $n_{ML}>1$

Two geometries also appear for n_{ML} larger than 1. The c/a ratios differ between the two geometries only by 10%–20% instead of the 44% found for $n_{ML}=1$. Pairing of the Pu planes (possible for $n_{ML}>1$) appears as the main difference between the two geometries. In Ref. 1, geometries with paired Pu planes were found when optimizing the Pb-Pu superlattices without allowing spin polarization (referred to here as "NM-paired"). Starting from these geometries and now allowing spin polarization increases the volume by 4%–6%, but otherwise changes the geometry negligibly, in particular, retaining the pairing ("AFM-paired"). The arising spin polarization lowers the energy, especially for odd n_{ML}. For even n_{ML}, the combination of Pu plane pairing and spin polarization results in energies lower than those obtained by spin polarization alone ("AFM-unpaired"). The AFM-unpaired systems remain lower in energy for odd n_{ML}.

Figure 4 plots these energies and the associated volumes. It reproduces the NM-paired and AFM-unpaired data plotted in the third figure of Ref. 1, but adds the AFM-paired phases. (Small changes in the values for the $n_{ML}=3$ NM-paired case reflect the finding of a state with slightly lower energy.) Pu atoms in the AFM-unpaired phases exhibit spin moments around $4.5\mu_B-5.2\mu_B$, while those in the AFM-paired phases display spin moments around $3.1\mu_B-3.5\mu_B$. These magnitudes differ from those found in calculations of α-Pu and are much closer to the values obtained for β-Pu.[28] The ratio of volumes for the AFM-paired to AFM-unpaired superlattices, ranging from 0.92 to 0.96, takes on values closer to those

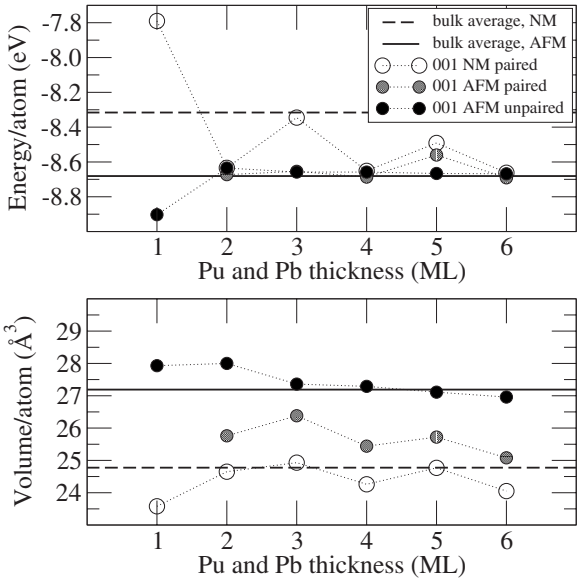

FIG. 4. Energies and volumes of (001)-direction Pb-Pu superlattices as a function of n_{ML} and imposed magnetic structure. The average energies and volumes stem from separate pure fcc Pu and pure fcc Pb calculations. Lines connecting the symbols are to guide the eye.

calculated relative to δ-Pu for β-Pu (0.93) and γ-Pu (0.98) than α-Pu (0.82).

The AFM-paired states reflect their NM-paired roots by reproducing some of the zigzag nature seen for the NM cases in both the energy and the volume as n_{ML} increases. Figure 4 reveals an exception: the $n_{ML}=3$ AFM-paired case's energy deviates from where one would expect to find it. Rather than lying near the middle between the values for the NM-paired and AFM-unpaired phases (as occurs for $n_{ML}=5$), the energy is only slightly (4 meV/atom per atom) higher than the AFM-unpaired energy. Symmetry breaking accounts for the exception: Without allowing spin polarization, no pairing of Pu planes occurs, but once spin polarization is allowed, the symmetry can be broken by pairing two Pu planes with small spin moments and having Pu atoms in the third plane pick up a large spin polarization. In other words, the Pu layer mixes both paired and unpaired phases. Section III C discusses this asymmetric pairing in detail. The corresponding asymmetric structure exists for $n_{ML}=5$ with an energy that lies 35 meV below that of the symmetric geometry, but still well above that of the AFM unpaired phase.

The remainder of this section compares the three systems with $n_{ML}=2$. The energies of the NM-paired and AFM-unpaired phases differ by a negligible amount, but the AFM-paired phase lies lower by 38 meV/atom. The AFM-unpaired and AFM-paired geometries appear in Fig. 1. The NM-paired geometry differs from the AFM-paired geometry in volume.

Figure 5 compares the electronic DOS for the three superlattice phases with $n_{ML}=2$. The AFM-unpaired phase exhibits a strongly peaked DOS near the Fermi level, associated with $5f$ electron states localized on the Pu sites, that appears mostly decoupled from a broad free-electron-like band originating around 4 eV below E_F, identifiable with the Pb $6p$ electron states. The two paired phases reveal less distinct

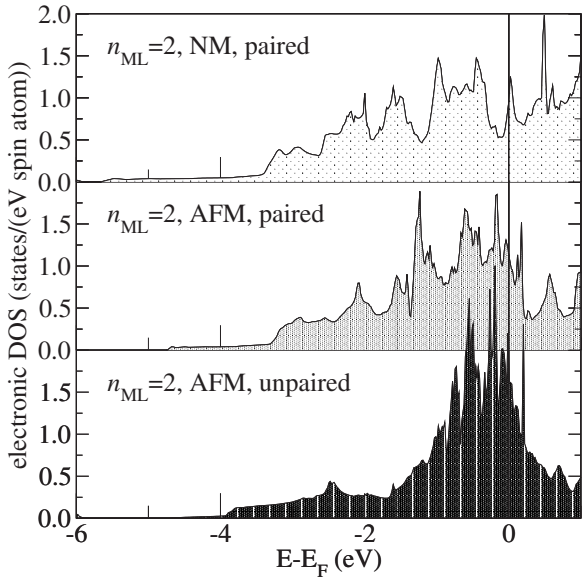

FIG. 5. Electronic DOS near the Fermi level for (001)-direction Pb-Pu superlattices with $n_{ML}=2$. The NM-paired and AFM-paired phases reveal very similar DOS despite having very different energies. The AFM-unpaired phase has an energy very close to that of the NM-paired phase, but shows a distinctly different DOS.

characteristics, with a broader band stemming from the Pu $5f$ states overlapping with much of the band with origins in Pb $6p$ states.

Figure 6 shows the band structure of the three superlattice phases with $n_{ML}=2$. Plotting the energy eigenvalues as they vary along the $(\xi,0,0)$ and $(0,0,\xi)$ directions in reciprocal space, i.e., perpendicular and parallel to the stacking direction, respectively, reveals significantly more dispersion perpendicular to the stacking direction, especially for the many states within 1–2 eV of the Fermi energy that stem from Pu $5f$ electrons. The superlattice geometry localizes the $5f$

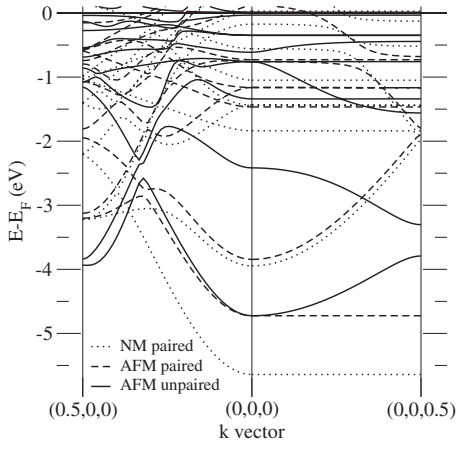

FIG. 6. Electronic band structure for (001)-direction Pb-Pu superlattices with $n_{ML}=2$ plotted perpendicular and parallel to the stacking direction. The two phases with paired-up Pu planes appear rather similar in character albeit somewhat shifted. The AFM phase without paired-up Pu planes takes on a different character, in particular, along the 001 direction.

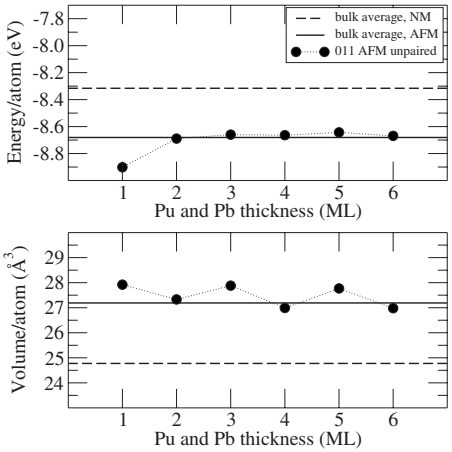

FIG. 7. Energies and volumes of (011)-direction Pb-Pu superlattices as a function of n_{ML} and imposed magnetic structure. The average energies and volumes stem from separate pure fcc Pu and pure fcc Pb calculations. Lines connecting the symbols are to guide the eye; energy and volume scales are kept the same as in the figures for the (001) and (111) directions.

electron states mainly parallel to the stacking direction. The effect of pairing on the localization of the $5f$ states appears in the number of such dispersion-muted states. For the unpaired geometry, four $(0,0,\xi)$-dispersion-free states appear, while for the paired geometries, only three emerge. Four (doubly occupied) $5f$ states appear in the superlattice phase corresponding to the bulk δ phase. This correlates well with results from the mixed level model, where the manifold with four localized $5f$ electrons describes the δ phase of bulk Pu in better agreement with experiment than other numbers of localized states.[18]

In summary, calculations predict two phases for Pb-Pu superlattices stacked in the (001) direction. One phase, energetically favored for odd n_{ML}, shows no pairing between Pu planes and large spin moments on the Pu atoms, implying localized $5f$ electron states. The other phase, energetically favored for even n_{ML}, pairs up neighboring Pu planes with smaller spin moments, indicative of less localized $5f$ electron states.

C. Variations with stacking direction

Figure 7 shows the calculated energies and volumes obtained for stacking in the (011) direction. The geometries of the AFM-unpaired phase remain close to that of an ideal fcc crystal with two atom types occupying the sites: The b/a ratios range from 1.26 to 1.4, compared to the ideal value of 1.42; the c/a ratios range from 0.96 to 1.09, close to the ideal value of unity. The energies hover around the bulk AFM average with little structure depending on even or odd n_{ML}. The entry for $n_{ML}=1$ does not distinguish between (001) and (011) directions. The geometry with $n_{ML}=2$ actually lies below the bulk average (by about 8 meV/atom). The volumes also approximate the bulk AFM average, but show more structure because of a weak pairing of Pu planes: the Pu-Pu bonds between closer neighboring planes are around

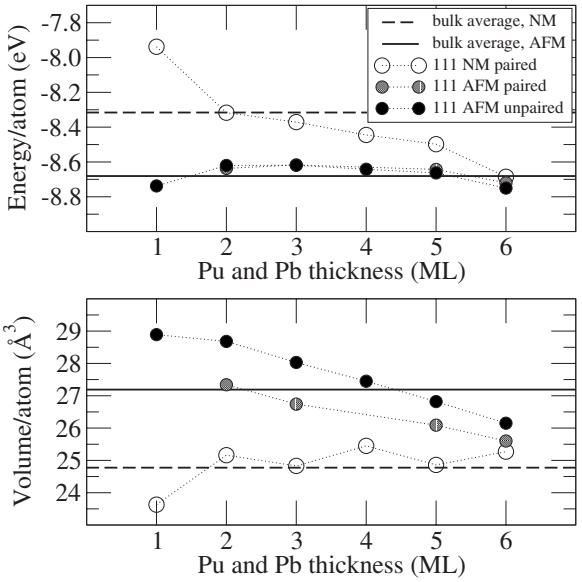

FIG. 8. Energies and volumes of (111)-direction Pb-Pu superlattices as a function of n_{ML} and imposed magnetic structure. The average energies and volumes stem from separate pure fcc Pu and pure fcc Pb calculations. Lines connecting the symbols are to guide the eye. The AFM-paired phase with $n_{ML}=4$ is missing because all optimizations allowing spin polarization ended in the AFM-unpaired phase.

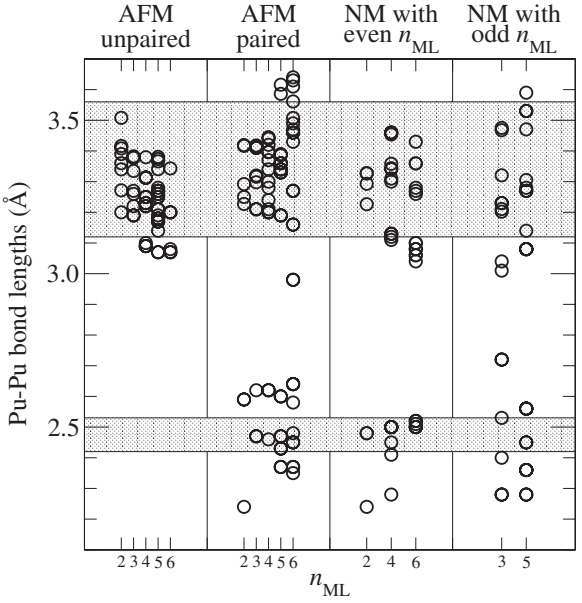

FIG. 9. Lengths of Pu-Pu bonds in Pb-Pu superlattices. Shaded regions represent lengths of so-called short bonds and long bonds found in α-Pu (theoretical values).

6% shorter than the Pu-Pu bonds between well-separated neighboring planes. This is significantly less than the around 20% value in the (001) AFM-paired geometries. This slight pairing is absent in the (001) direction.

Unlike for the (001) direction in Fig. 4, no paired geometries appear for the (011) direction in Fig. 7. For every n_{ML}, all geometries with paired Pu planes stacked in the (011) direction, i.e., with $a \neq b$, consistently relaxed to $a=b$ and reproduced the (001) results. Calculations with $n_{ML}=2$ suggest why: On the one hand, the energy increases for a volume-conserving distortion that decreases the b/a ratio of the AFM-unpaired geometry, with $n_{ML}=2$ stacked in the (011) direction. On the other hand, the same distortion decreases the energy if the two Pu planes are paired up. In short, pairing destabilizes the geometries of Pb-Pu superlattices stacked in the (011) direction with respect to the geometries of superlattices stacked in the (001) direction.

Figure 8 shows the calculated energies and volumes obtained for stacking in the (111) direction. Stacking in this direction lowers the symmetry more than for the previous two directions. Pairing of Pu planes becomes less pronounced. Visible systematic differences between odd and even n_{ML} only appear for the volumes of the NM-paired phase, with even n_{ML} showing larger volumes than odd n_{ML} [opposite to the ordering in the (001) direction]. As n_{ML} increases, the geometries tend toward that of bulk α-Pu sandwiched between fcc Pb as do the energy and volume: the average energy and volume of pure bulk α-Pu and fcc Pb are −8.83 eV/atom and 24.7 Å^3, respectively.

Figure 9 collects the Pu-Pu bond lengths that appear in Pb-Pu superlattices for all three stacking directions and compares them to the ranges of short and long bonds found in the α phase of bulk Pu. The bond lengths for the AFM-unpaired phase all fall close to the range of long α-Pu bonds, where the bond length of bulk fcc Pu also lies. The AFM-paired phase reveals a splitting into short and long bonds similar to that found in bulk α-Pu. The NM results show this splitting to the degree that pairing succeeds, i.e., more clearly for even n_{ML} where all Pu planes can pair up.

In summary, calculations predict two phases for Pb-Pu superlattices stacked in the (111) direction as seen for stacking in the (001) direction. For stacking in the (011) direction, only the unpaired phase appears, because pairing Pu planes destabilizes the crystal structure with respect to a shearing of the base plane that converts the structures into the geometry of the (001)-direction paired phase. With increasing layer thicknesses, the (111)-direction superlattices tend toward the appearance of bulk α-Pu's geometry within the Pu layer.

D. Asymmetric pairing in the $n_{ML}=3$ case

The (001) Pb-Pu superlattice with $n_{ML}=3$ deserves particular scrutiny as it exhibits the $5f$ electron itinerant-localized transition in a unique setting. Without spin polarization, breaking the spatial symmetry to allow two neighboring Pu planes to pair up raises the energy. With spin polarization, the symmetry in spin can be broken and two solutions appear as for other values of n_{ML}. The first solution lowers the energy by acquiring large spin moments near $5\mu_B$, i.e., localized $5f$ electron states, at the Pu sites without pairing of Pu planes. The second solution lowers the energy with spatial symmetry breaking made possible by spin polarization: two Pu planes (with small spin moments near $3\mu_B$) pair up, while the remaining Pu atom takes on a larger spin moment over $5\mu_B$. This arrangement combines both the paired and unpaired phases in the same Pu layer. Figure 10 illustrates the geometry of this asymmetric pairing.

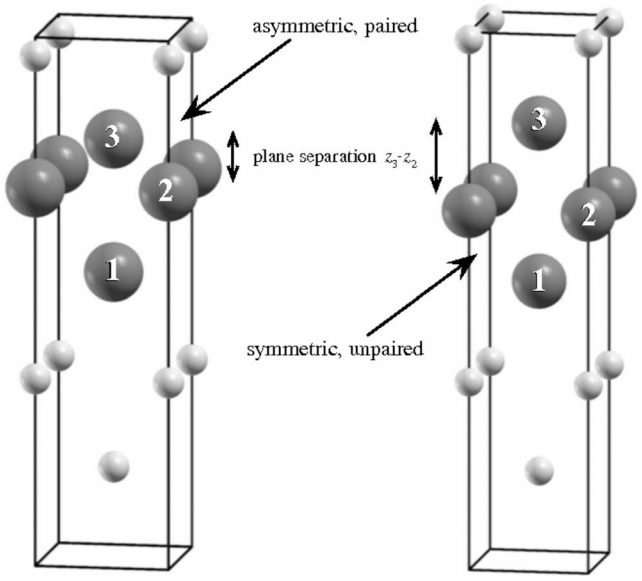

FIG. 10. Unit cell geometries of the (001) $n_{ML}=3$ Pb-Pu superlattice in the asymmetric pairing phase (left) and in the symmetric unpaired phase (right). The transition is accompanied by a slight volume change from 26.38 to 27.37 Å^3, and a change in c/a ratio from 0.93 to 1.06. Spin moments are negative on atoms 1 and 3, and positive on atom 2.

The unpaired phase with its high degree of symmetry and large spin moments emulates the bulk δ-Pu phase. The paired phase emulates several bulk Pu phases in different aspects or, as mentioned above, emulates two bulk phases simultaneously by combining both paired and unpaired superlattice phases. This combined concept receives support from the magnitudes of the spin moments, with values emulating the bulk γ-Pu and δ-Pu phases. The splitting of Pu-Pu bond lengths into two groups mirrors the bulk α-Pu phase. The entire superlattice system's calculated bulk modulus changes from 29.0 GPa (unpaired) to 34.9 GPa (paired); these values are closer to the 33 GPa calculated[28] for γ-Pu than any of the other phases. While the asymmetry of the paired phase raises the notion of viewing it as loosely connected sublayers, the usefulness of this concept remains debatable.

The usefulness of the simple geometric path connecting the two phases becomes apparent immediately: Fixing the geometry at points that linearly interpolate the path connecting the two spin-polarized phases allows the transition between them to be mapped out. Figure 11 plots the continuous changes arising in the transition between the two $n_{ML}=3$ phases. Slight extensions at both ends of the path connecting the unpaired and paired phases reveal the two distinct energy minima. The paired geometry's energy lies 4 meV/atom higher than that of the unpaired phase. The energy barrier separating the two geometries, 29 meV/atom, only slightly exceeds room temperature, making this transition quite possible. The symmetry of the unpaired phase reappears in both the spin moments and the bond lengths between Pu atoms in neighboring planes; both of these entities reveal no particular structure at the asymmetric, paired phase.

Unlike the energy, the spin moments change monotonically as the geometry progresses monotonically from one

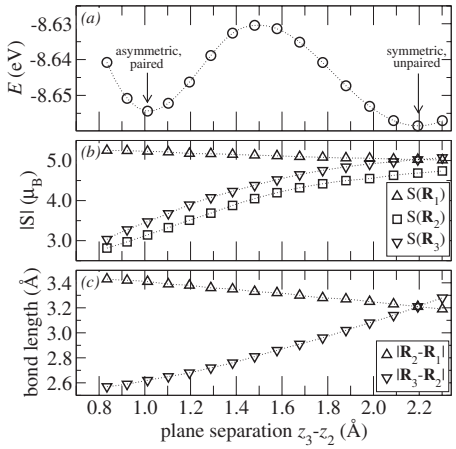

FIG. 11. Energy, spin moments, and bond lengths along the transition path connecting symmetric unpaired and asymmetric paired phases in (001) $n_{ML}=3$ Pb-Pu superlattice. The plane separation z_3-z_2 corresponds to the geometry illustrated in Fig. 10.

phase to the other. This parallelism between geometry and electronic state demonstrates a distinct link between the localization of 5f electron states and Pu-Pu bond lengths. Only when the superlattice geometry suddenly changes will the localization suddenly change. This continuous variation of spin moment with local geometry similarly appears in the bulk phases of Pu.[28]

Figure 12 shows the projected electronic DOS of the three Pu atoms at three states along the path: the paired and unpaired phases as well as the intermediate maximum-energy

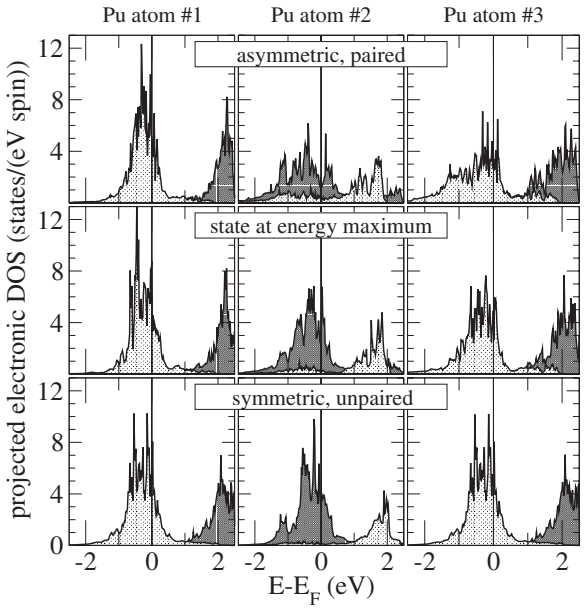

FIG. 12. Projected f-character electronic DOS for points on the transition path connecting symmetric unpaired and asymmetric paired phases in (001) $n_{ML}=3$ Pb-Pu superlattice. The Pu atoms are numbered as in Fig. 10, i.e., atoms 2 and 3 partake in the pairing. The three geometries correspond to the local energy minima and maximum in Fig. 11. The two different shadings correspond to spin directions with atoms 1 and 3 showing spin down at E_F.

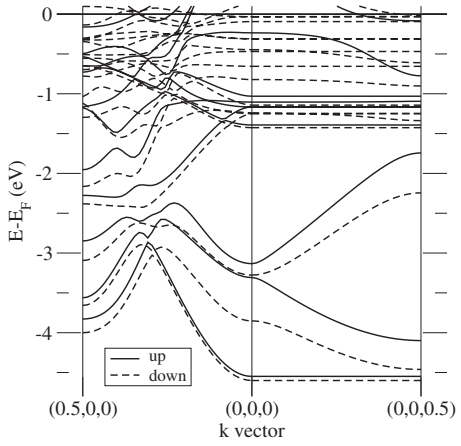

FIG. 13. Band structure along high-symmetry directions for the asymmetric paired phase in (001) $n_{ML}=3$ Pb-Pu superlattice.

state. Very little change appears in the projected DOS of the atom that remains unpaired (Pu atom No. 1) as its spin moment only slightly decreases. On the other hand, the spin moments increase steadily for the two Pu atoms participating in pairing, and their $5f$ electron states become more localized and the projected DOS become more peaked just below the Fermi energy.

The bunching up of $5f$ electron states near the Fermi energy emerges in the band structure. Figures 13 and 14 show the band structures along high-symmetry directions for the asymmetric paired and symmetric unpaired phases, respectively. Two of the three Pu atoms have a negative spin moment, while the middle Pu atom has a positive spin moment, resulting in more spin-down than spin-up bands below the Fermi energy. Many of the effects due to Pu plane pairing and $5f$ electron localization seen in Fig. 6 also become apparent here. The symmetric unpaired phase reveals its more localized $5f$ electron states bunched up just below the Fermi energy and with no dispersion in the stacking direction. The $5f$ electron states, being more localized in the unpaired phase, also couple less to other states. Consequently, the structure stemming from the Pb $6p$ states appears more free-electron-like as in the $n_{ML}=2$ band structure.

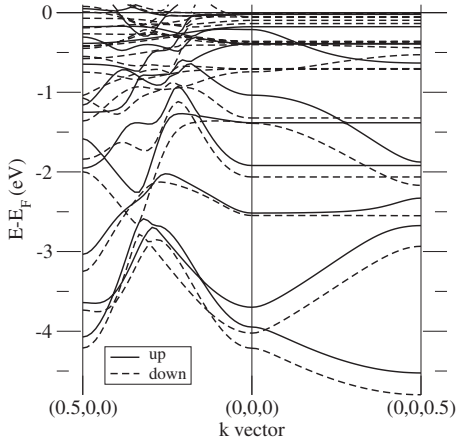

FIG. 14. Band structure along high-symmetry directions for the symmetric unpaired phase in (001) $n_{ML}=3$ Pb-Pu superlattice.

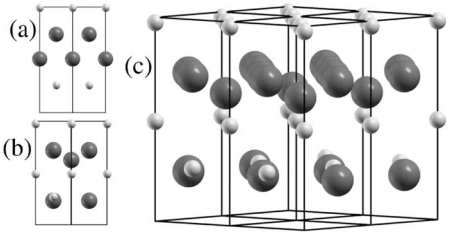

FIG. 15. Geometry of Pb-Pu superlattice with $n_{ML}=2$ including interface alloying. (a) Original AFM $n_{ML}=2$ unit cell as seen from the (110) direction. The alloying at the interface is created by exchanging the edge Pu atom with the Pb atom in the front right face (and, equivalently, the back left face). (b) Relaxed unit cell from the same viewpoint, showing how the center Pu atom has moved up to pair with the pure Pu plane. (c) Relaxed unit cell viewed from angle. Small and large spheres represent Pb and Pu atoms, respectively; rods delineate the simulation cells. The spin moments at the Pu sites are −5.26 (bottom, mixed layer), 3.30 (moved-up layer), and 4.67 and −4.50 in the slightly buckled topmost layer.

In summary, an exploration of the path connecting the two phases for $n_{ML}=3$ reveals a distinct link between the Pu-Pu bond lengths and the degree of $5f$ localization. The degree of $5f$ localization can, in fact, vary across the Pu layer as superlattices with odd numbers of monolayers allow for geometries that combine both the paired and unpaired phases in the same Pu layer.

E. Interface stability and alloying

The calculated energies of (001) Pb-Pu superlattices with n_{ML} larger than unity lie 20–60 meV/atom above the average of the two bulk fcc structures. In contrast, the energy calculated for $n_{ML}=1$, corresponding to the alloy in a tetragonally distorted B2 structure, lies around 200 meV/atom lower than the bulk fcc average. The favoring of the alloy suggests that Pb-Pu superlattices with n_{ML} larger than unity might be stabilized by blending the two elements across the interface. A complete, systematic exploration of this issue goes beyond the scope of this paper.

Evidence for such interface alloying appears in one case presented in this section. Figure 15 shows the optimized geometry. The initial geometry derives from the optimized $n_{ML}=2$ superlattice by exchanging one row of Pb with one row of Pu atoms to create a mixed layer. The optimized volume decreases from the original AFM-unpaired phase by 4%. The energy becomes more favorable by 124 meV per atom, but remains higher than the $n_{ML}=1$ superlattice. The optimized geometry can be viewed as two Pb monolayers separated by a layer of Pu in the AFM-paired phase and a layer of PbPu alloy.

In summary, the optimized $n_{ML}=2$ (001) Pb-Pu superlattice can be stabilized by introducing interface alloying.

IV. CONCLUSION AND DISCUSSION

In conclusion, DFT calculations in the GGA allowing spin polarization reveal two phases for Pb-Pu superlattices that closely emulate many characteristics of the low- and high-

temperature phases of bulk Pu. Aspects of the phase transition that reveal the resemblance appear in the localization of $5f$ electron states, a large change of volume, and Pu-Pu bonds of similar lengths. In bulk, Pu settles in phases that either increase the localization of $5f$ electron states or exhibit low crystal symmetry. The superlattice shows the same trend, though the $5f$ electron states localize mainly in one dimension, parallel to the stacking direction. The lowering of crystal symmetry also proceeds less dramatically.

The lesser lowering of symmetry stems from the Pu layer's being embedded between Pb layers. For the Pu atoms at the interface of superlattices with stacking along the (001) and (011) directions, Pb provides a potential that encourages a structure that is more like δ-Pu than α-Pu. Keeping the high degree of symmetry imparted across the interface constrains the distortion of the Pu layer to the pairing up of planes. While the pairing up does not lower the symmetry to that of α-Pu, it does yield the same splitting into short and long Pu-Pu bonds found in α-Pu.

The pairing up of Pu planes appears less pronounced for stacking in the (111) direction. The lower symmetry at the interface provides less constraints on the distortion of the Pu layer's lattice structure.

The pairing up of Pu planes connects the two superlattice phases through a distinct transformation. The simple geometry of the pairing allows for detailed calculations exploring the transition along the complete path connecting the two phases, an investigation that, to date, is not possible for the bulk phases. Evidence for a continuous change of $5f$ electron localization with geometry, found in bulk Pu phases, emerges with clarity in calculations along the superlattice transformation.

The PbPu alloy in a tetragonally distorted B2 structure lies lower in energy than the thicker Pb-Pu superlattices. The stability of this crystal structure suggests that chemical short-range-order effects may be important and that alloying may occur at the superlattice interfaces. Further investigations are needed, but a test calculation reveals evidence for the stabilization of superlattices by such blending of the elements across the interface.

The calculations presented here presumably reflect a small selection of the effects of nanometer-scale confinement on plutonium. In addition to introducing elements other than Pb, exploring other stoichiometries or other geometries may well reveal more insight into the nature of Pu.

ACKNOWLEDGMENTS

This research was supported by the U.S. Department of Energy under Contract No. W-7405-ENG-36. Many thanks go to John Wills for helpful and encouraging discussions.

[1] S. P. Rudin, Phys. Rev. Lett. **98**, 116401 (2007).
[2] *The Chemistry of the Actinide Elements*, edited by L. R. Morss, N. M. Edelstein, and J. Fuger (Springer, Dordrecht, 2006).
[3] B. Johansson, Philos. Mag. **30**, 469 (1974).
[4] B. Johansson, Phys. Rev. B **11**, 2740 (1975).
[5] H. L. Skriver, O. K. Andersen, and B. Johansson, Phys. Rev. Lett. **41**, 42 (1978).
[6] S. Méot-Reymond and J. M. Fournier, J. Alloys Compd. **232**, 119 (1996).
[7] P. de V. du Plessis, G. H. Lander, A. M. Strydom, and B. Fåk, Physica B **180-181**, 321 (1992).
[8] J.-C. Marmeggi, G. H. Lander, R. Currat, and C. M. E. Zeyen, Physica B **234-236**, 129 (1997).
[9] M. E. Manley, B. Fultz, R. J. McQueeney, C. M. Brown, W. L. Hults, J. L. Smith, D. J. Thoma, R. Osborn, and J. L. Robertson, Phys. Rev. Lett. **86**, 3076 (2001).
[10] R. J. McQueeney, A. C. Lawson, A. Migliori, T. M. Kelley, B. Fultz, M. Ramos, B. Martinez, J. C. Lashley, and S. C. Vogel, Phys. Rev. Lett. **92**, 146401 (2004).
[11] M. J. Graf, T. Lookman, J. M. Wills, D. C. Wallace, and J. C. Lashley, Phys. Rev. B **72**, 045135 (2005).
[12] D. H. Wood, E. M. Cramer, P. L. Wallace, and W. J. Ramsey, J. Nucl. Mater. **32**, 193 (1969).
[13] J. Dognon, C. Clavaguera, and P. Pyykkö, Angew. Chem., Int. Ed. **46**, 1427 (2007).
[14] T. Gouder, L. Havela, F. Wastin, and J. Rebizant, Europhys. Lett. **55**, 705 (2001).
[15] P. Hohenberg and W. Kohn, Phys. Rev. **136**, B864 (1964).
[16] W. Kohn and L. J. Sham, Phys. Rev. **140**, A1133 (1965).
[17] D. C. Langreth and J. P. Perdew, Phys. Rev. B **21**, 5469 (1980).
[18] O. Eriksson, J. D. Becker, A. V. Balatsky, and J. M. Wills, J. Alloys Compd. **287**, 1 (1999).
[19] J. P. Perdew and A. Zunger, Phys. Rev. B **23**, 5048 (1981).
[20] L. Petit, A. Svane, W. M. Temmerman, and Z. Szotek, Solid State Commun. **116**, 379 (2000).
[21] V. I. Anisimov, J. Zaanen, and O. K. Andersen, Phys. Rev. B **44**, 943 (1991).
[22] J. Bouchet, B. Siberchicot, F. Jollet, and A. Pasturel, J. Phys.: Condens. Matter **12**, 1723 (2000).
[23] S. Y. Savrasov and G. Kotliar, Phys. Rev. Lett. **84**, 3670 (2000).
[24] S. Y. Savrasov, G. Kotliar, and E. Abrahams, Nature (London) **410**, 793 (2001).
[25] A. V. Postinov and V. P. Antropov, Comput. Mater. Sci. **17**, 438 (2000).
[26] Y. Wang and Y. Sun, J. Phys.: Condens. Matter **12**, L311 (2000).
[27] A. M. N. Niklasson, J. M. Wills, M. I. Katsnelson, I. A. Abrikosov, O. Eriksson, and B. Johansson, Phys. Rev. B **67**, 235105 (2003).
[28] P. Soderlind and B. Sadigh, Phys. Rev. Lett. **92**, 185702 (2004).
[29] J. C. Lashley, A. Lawson, R. J. McQueeney, and G. H. Lander, Phys. Rev. B **72**, 054416 (2005).
[30] G. Robert, A. Pasturel, and B. Siberchicot, Phys. Rev. B **68**, 075109 (2003).
[31] B. Sadigh and W. G. Wolfer, Phys. Rev. B **72**, 205122 (2005).
[32] G. Robert, C. Colinet, B. Siberchicot, and A. Pasturel, Philos. Mag. **84**, 1877 (2004).
[33] P. E. Blöchl, Phys. Rev. B **50**, 17953 (1994).
[34] G. Kresse and J. Furthmuller, Phys. Rev. B **54**, 11169 (1996).

[35] G. Kresse and D. Joubert, Phys. Rev. B **59**, 1758 (1999).
[36] J. P. Perdew, J. A. Chevary, S. H. Vosko, K. A. Jackson, M. R. Pederson, D. J. Singh, and C. Fiolhais, Phys. Rev. B **46**, 6671 (1992).
[37] J. P. Perdew, J. A. Chevary, S. H. Vosko, K. A. Jackson, M. R. Pederson, D. J. Singh, and C. Fiolhais, Phys. Rev. B **48**, 4978(E) (1993).
[38] P. E. Blöchl, O. Jepsen, and O. K. Andersen, Phys. Rev. B **49**, 16223 (1994).
[39] K. Kunc and R. M. Martin, Phys. Rev. Lett. **48**, 406 (1982).
[40] S. Wei and M. Y. Chou, Phys. Rev. Lett. **69**, 2799 (1992).
[41] W. Frank, C. Elsasser, and M. Fahnle, Phys. Rev. Lett. **74**, 1791 (1995).
[42] K. Parlinski, Z.-Q. Li, and Y. Kawazoe, Phys. Rev. Lett. **78**, 4063 (1997).